Depletion-Induced Chiral Chain Formation of Magnetic Spheres.

Sandrine Heijnen

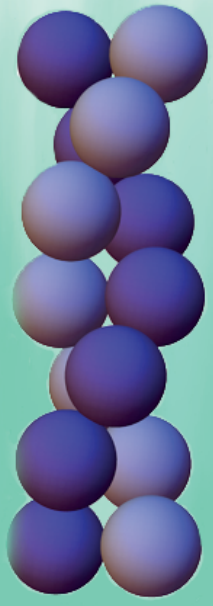

Utrecht University

VAN 'T HOFF LABORATORIUM

Master Thesis

Depletion-Induced Chiral Chain Formation of Magnetic Spheres.

Sandrine M. F. Heijnen

under supervision of:

Dr. S. Ouhajji

prof. A.P. Philipse

Dr. A.V. Petukhov

Van 't Hoff laboratory
for
Physical and Colloid Chemistry
Utrecht University

July 31, 2019

Abstract

Simulations by Pickett et al. predict that aligned spherical particles with a dipole moment can self-assemble into helical structures in the presence of an additional attractive interaction. This prediction was experimentally tested employing superparamagnetic silica spheres and depletion polymer polyethylene oxide. A Helmholtz cube was used to produce a homogeneous magnetic field. The observed structures of the arised single and double chains were analysed by optical microscopy within a homogeneous magnetic field. The behaviour of superparamagnetic silica particles in the presence of PEO was characterized by determining chain length, amount of double chains and the rotation of the double chains. Additionally, photo-crosslinkable surface-modified superparamagnetic silica particles were used to attempt to fixate the structures because the structures will fall apart without the magnetic field.

Contents

Chapter 1

Introduction

Colloids are particles with a size ranging from a few nano- to a couple of micrometres. These particles play an important role in fundamental research because they are visible with optical microscopy but still have Brownian motion, Brownian motion is the random motion due to thermal energy [1]. They are considered a model system for atoms because both display Brownian motion [2]. In this research colloids are used as model system to construct chiral structures. A structure is considered chiral if the its image in a mirror plane cannot be brought to coincide with itself [3]. This includes components like a DNA double helix and structural isomers.

Examples in literature can be found where chiral structures are formed from magnetic particles. For example Yan et al. showed that a system of partially magnetically functionalised spheres, Janus particles, can self assemble in a dynamical chiral structure when a magnetic field is switched on. Dependent on the precision angle, that describe the motion dependent on rotation and oscillation frequency of the particles and coating thickness, distinctive chiral structures would form, see Figure 1.1a [4]. Experiments by Zerrouki et al. showed that chiral structures were formed by modifying the shape of the magnetic particles. Dependent on the size ratio of the dumbbell shaped magnetic particles, different structures formed if these particles were exposed to a magnetic field, see Figure 1.1b [5].

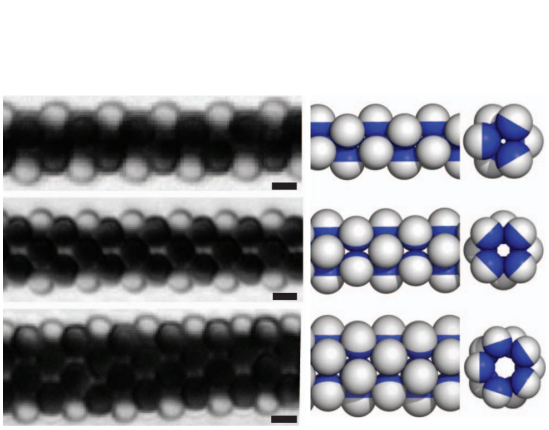

(a) Chiral structures from Janus particles. The Janus particles have different precision angles that determine the kind of chiral structure.[4]

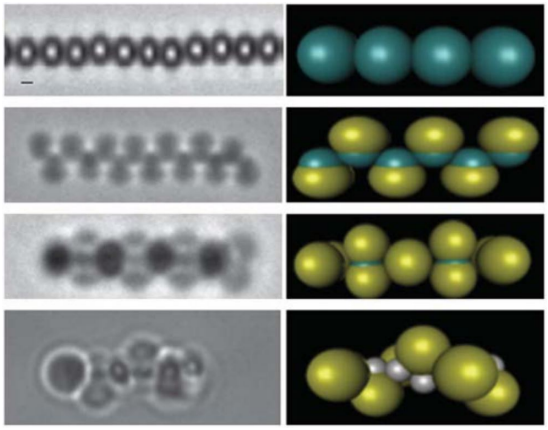

(b) Chiral structures from partially magnetic dumbbells. The size ratio of the dumbbells determine the kind of structure. [5]

Figure 1.1: Two experimental examples of constructing chiral structures from magnetic colloids.

However, it was predicted by Pickett et al. that no anisotropic magnetic particles are required to form chiral structures. The simulations were presented to show the sponta-

neous formation of symmetry breaking structures. The article predict that aligned spherical particles with a dipole moment can form helical chains in the presence of an additional attractive interaction. In the paper they state the following "An approximate example of such a system consists of magnetorheological (MR) particles with additional shortranged, attractive interactions generated by the addition of smaller particles." [6]. Their prediction could be experimentally tested employing superparamagnetic spheres and polymer. The polymer acts as a particle with a radius of gyration and gives rise to the depletion interaction. This situation is visualised in Figure 1.2. An example of this system consists of superparamagnetic silica colloids and polyethylene oxide.

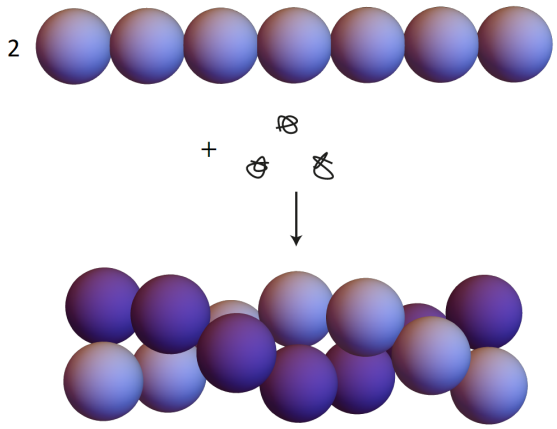

Figure 1.2: A visualisation of aligned spherical particles with a dipole moment that form helical chains upon the addition of smaller particles.

In this thesis the focus will be on the formation of chiral structures from uniform magnetic particles. The method to produce these structures is based on a simulation done by Pickett et al. where chiral structures will form in the right circumstances [6]. Preliminary experiments were preformed that showed an attempt to create helical structures from uniform magnetic particles and fixate them. Chains twisting around each other and clusters were found, as can be seen in Figure 1.3a. An attempt of fixating the structures, so the structures would not fall apart if the magnetic field was turned off, resulted in clusters, see Figure 1.3b. The flaw within these experiments was the use of magnetic field induced by two small magnets [7]. These magnets will not provide a homogeneous field. These experiments will be reproduced with a homogeneous magnetic field.

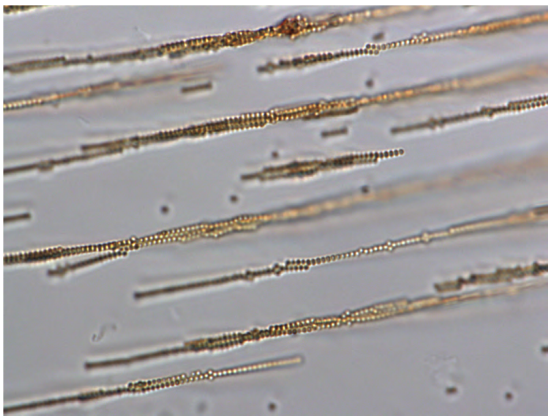

(a) Twisiting of superparamagnetic silica spheres around each other.

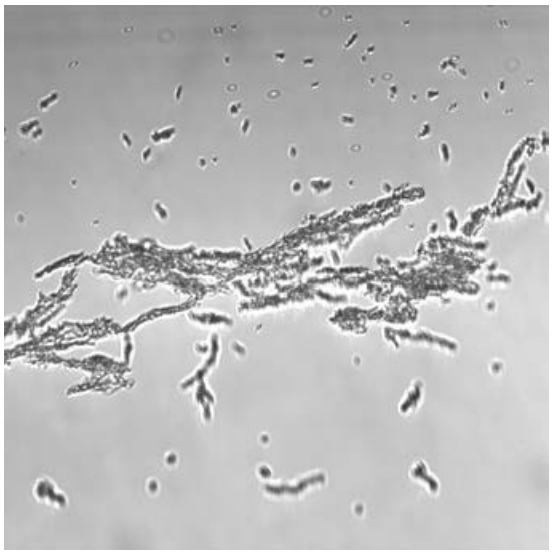

(b) An attempt of fixating the twisting chains, resulted in these clusters.

Figure 1.3: Preliminary results of experimentally probing the prediction by Pickett et al. by employing magnetic silica spheres and polymer polyethylene oxide to a magnetic field [7].

Chapter 2

Theory

2.1 Depletion Interaction

Depletion interaction can come into play when a system contains colloids and a depletant. This interaction can be explained by comparing it to a practical situation. Imagine the following: a dining room of a restaurant filled with tables and people. On a regular night, the tables will be distributed through the room and all the people have a place to sit. During a special occasion, like a birthday party, there will be more people present than chairs available. The set up of the room will be changed where the tables will be placed against the wall and a large space opens up. This situation is visualized in Figure 2.1. This is comparable to what happens in a system of colloids where a depletant is added. At a certain depletant concentration it is energetically more favourable for the colloids to cluster together because the free space for the depletant will increase. This is due to the overlap of the excluded volumes. The excluded volume is defined as the distance at which the centre of the depletant cannot be present. Clustering of the colloids will therefore decrease the energy of the system [8]. Depletion interaction in visualized in Figure 2.2. A rough estimation of the strength of the depletion interaction can be calculated the force method which relies on the Derjaguin approximation.

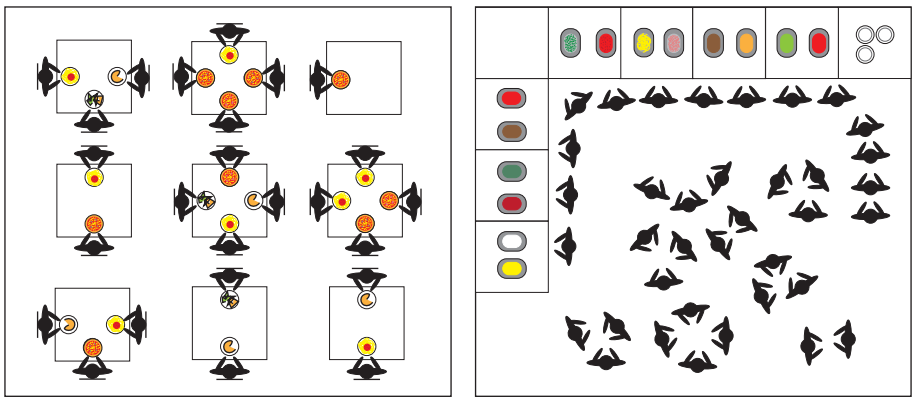

Figure 2.1: A visualisation of a restaurant with on the left the set up on a regular night and on the right during a special occasion. Adapted from H. Lekkerkerker and R. Tuinier. [8].

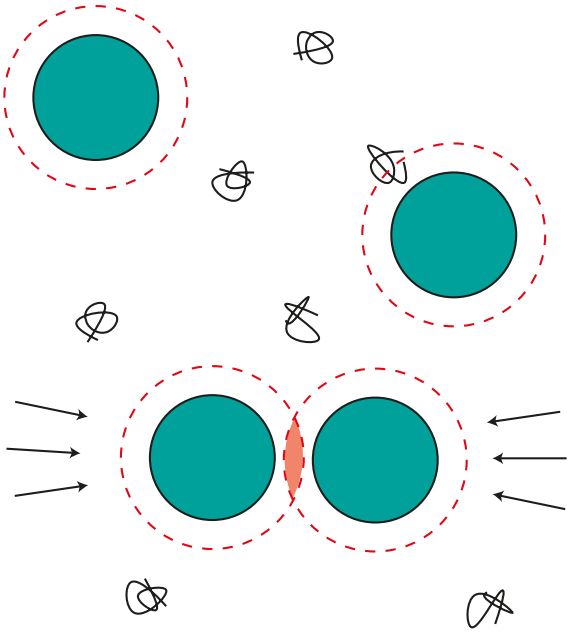

Figure 2.2: A visualisation of depletion interaction where the excluded volume of the colloids is indicated with a red dotted line, the overlap of the excluded volume is indicated in red and the arrows indicate the resulting force pushing the particles further together.

2.1.1 Derjaguin Approximation

The Derjaguin approximation relates the force between two curved objects to the interaction potential between two flat plates. The Derjuguin approximation replaces the spherical surface of the two curved objects by a collection of flat rings. This approximation with the relevant length scales is visualized in Figure 2.3. The centre-to-centre distance between two spheres is the sum of the radius, R, and the distance in between the spheres, h. At different heights, z, of the sphere the distance in between the particles, H, is equal to

$$H = h + 2\Delta. \tag{2.1}$$

The distance Δ, indicated in Figure 2.3 for $z \ll R$, can be defined as

$$\Delta = z^2/2R. \tag{2.2}$$

This definition, Equation 2.2, combined with the expression for the distance in between the spheres at different heights, Equation 2.1, and a derivation over the path length results in

$$dH = 2zR^{-1}dz. \tag{2.3}$$

The interaction potential of two spheres, W_s, is defined as the interaction potential of a plate integrated over a sphere,

$$W_s(h) = \int_0^\infty W_p(H)2\pi z dz. \tag{2.4}$$

Equation 2.3 can be substituted into Equation 2.4 to obtain the expression for the interaction energy between two spheres,

$$W_s(h) = \pi R \int_h^\infty W_p(H)dH \tag{2.5}$$

[8].

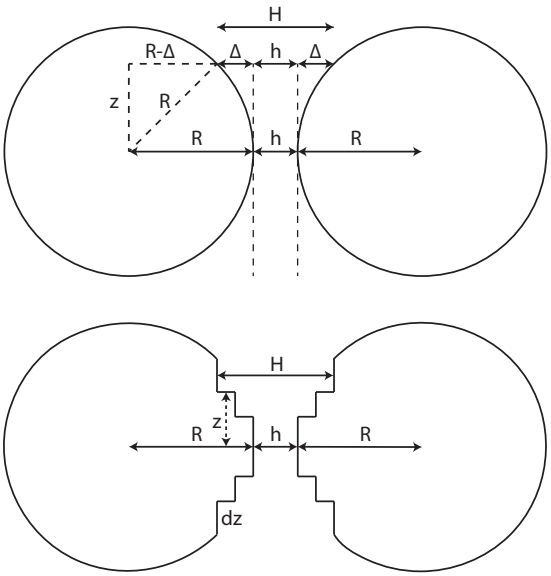

Figure 2.3: A visualisation of the relevant length scales in the Derjaguin approximation. Top: the spheres are visible. Bottom: the spheres are seen as a collection of flat rings. Adapted from H. Lekkerkerker et al. [8].

2.1.2 Force Method

The strength of the depletion interaction can be calculated with the force method. This method relies on the idea that for two plates with no depletant between them, the depletant concentration difference will push the plates closer together. Absence of depletant between the plates can occur when the distance between the plates is smaller than the depletant size. The total force on the plates is equal to the difference in pressure in between the plates and outside,

$$K(h) = P_i - P_0. \tag{2.6}$$

Here, K is defined as the total force, h as the distance between two plates, P_i as the pressure between the plates and P_0 as the pressure outside the plates. This situation is visualized in Figure 2.4. The pressure of the dispersion of an ideal solution is equal to osmotic pressure as defined by Van 't Hoff's Law,

$$P_0 = -n_b k_b T. \tag{2.7}$$

In this equation n_b is defined as the molar concentration of depletant, k_b as the Boltzmann constant and T as the temperature. If the distance between the plates is smaller or largers than the depletant size the pressure and corresponding force can be calculated,

$$\begin{aligned} \text{if } h < \sigma : P_i = 0 \qquad & K = -n_b k_b T \\ \text{if } h > \sigma : P_i = P_0 \qquad & K = 0. \end{aligned} \tag{2.8}$$

In these equations σ is the depletant size. The pressure is related to the interaction energy,

$$W_p(h) = \int_{\infty}^{h} K dh \tag{2.9}$$

Equation 2.9, by the integration over the distance in between the plates, h. In this equation W_p is the interaction energy between the plates. The interaction energy can also

be calculated for the two situations,

$$\begin{aligned} \text{if } h < \sigma: \; W_p(h) &= \int_h^\sigma -n_b k T dh \\ W_p(h) &= [-n_b k_b T h]_h^\sigma \\ W_p(h) &= -n_b k_b T(\sigma - h) \end{aligned} \tag{2.10}$$

$$\text{if } h > \sigma: \; W_p(h) = 0. \tag{2.11}$$

Equation 2.11 shows that the pressure indeed only occurs when the distance in between the plates is smaller than the depletant size. To obtain the depletion interaction between two spheres the Degajuin approximation, Equation 2.5, will be combined with the interaction calculated in between two plates, Equation 2.10,

$$W_s(h) = \int -n_b k_b T \pi R(\sigma - h) dH. \tag{2.12}$$

The depletion interaction can now be calculated with this expression. For simplicity the result of integrating over the depletion overlap zone

$$W_s(h) = \frac{-n_b k_b T \pi R}{2}(\sigma - h)^2 \tag{2.13}$$

is also provided. Using the expression derived by the force method the depletion interaction at contact was calculated for the superparamagnetic silica particles to be -2.51 kT [8].

2.2 Dipolar Hard Sphere Interaction

The dipolar hard sphere (DHS) interaction is the attraction or repulsion between two hard spheres due to their dipole moment. The DHS interaction is at a maximum when two hard spheres are vertically aligned with their embedded dipole, as in Figure 2.5 [9]. The dipolar hard sphere interaction in this situation can be calculated

$$w(r) = -\frac{2\mu_0 \mu^2}{4\pi k T d^3}. \tag{2.14}$$

Here, μ_0 being the vacuum permeability, μ the dipole moment of the spheres and d the diameter of the spheres [10, 11]. The dipole hard sphere interaction for two superparamagnetic spheres with a diameter of 510 nm is -2.8 kT.

2.3 Gravitational Length

The gravitational length is a measure of the balance between the thermal energy and the gravitational force. According to Buzzaccaro et al. the gravitational length is defined as "The distance a particle has to settle before the sedimentation drift becomes equal to the root mean square displacement due to Brownian motion"[12]. This means that the gravitational length needs to be large enough to get all the particles at the bottom of the sample and the depletion interaction and magnetic dipole might not be able to form the alleged structures. The gravitational length, L_g, can be calculated with

$$L_g = \frac{kT}{\frac{4}{3}\pi R^3 \Delta\rho g}. \tag{2.15}$$

Here, $\Delta\rho$ is the difference in density between the particles and the medium [13]. For superparamagnetic silica spheres with a diameter of 510 nm the gravitational length is 2.5 micrometer.

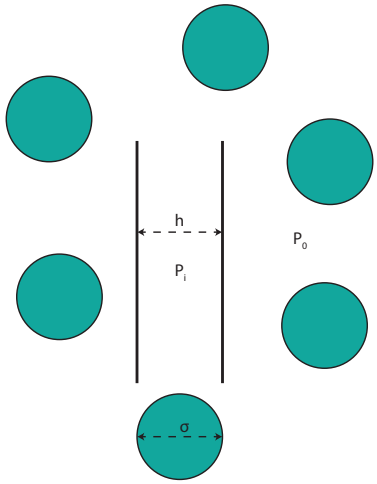

Figure 2.4: The visualisation of plates and the depletant, represented by spheres, where the distance in between the plates limits the region accessible for the depletant.

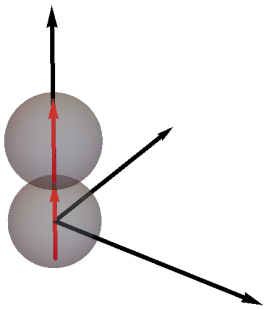

Figure 2.5: A visualisation of two particles with an aligned dipole.

2.4 Superparamagnetic Colloids

Superparamagnetic colloids contain small nanoparticles with a magnetic moment that can change direction randomly due to thermal energy. Applying a magnetic field will orient the magnetic moment of the particles to the applied field, if the magnetic field is strong enough to overcome the thermal agitation. The magnetisation of the particles can be tuned with the strength of the magnetic field. A stronger magnetic field will give an increase in the magnetic moment of the particles until the saturation value [14].

2.5 Coumarin Click Reaction

The ability to freeze structures in the sample means that the structures could be analysed without a magnetic field and their self assembly. A method that could be used is coumarin functionalised particles. Coumarin is a photoresponsive molecule that can photodimerize upon irradiation with UV light with a wavelength 365 nm forming a cyclobutane ring between adjacent double bonds, visualized in Figure 2.6 [7].

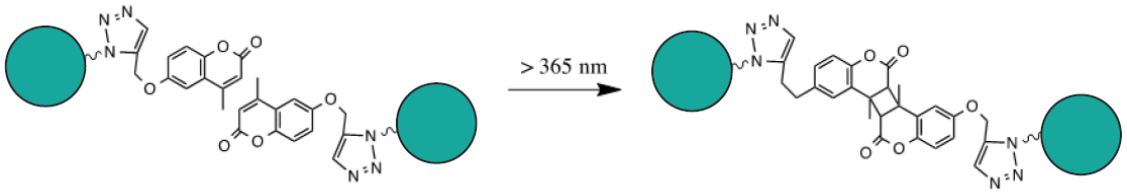

Figure 2.6: A visualisation of two particles with coumarin on the surface photodimerizing together when exposed to UV light.

2.5.1 ATRP Reaction

The atomic transfer radial polymerization (ATRP) reaction is used to grow polymers. It can also be used to grow polymer hairs on a surface, also known as surface-initiated ARTP reaction. To preform an ATRP reaction, three components must be present, namely a catalyst, an initiator with a transferable (pseudo)halogen and a suitable monomer. There are two vital steps in a ATRP reaction. The first step results in a radical on the surface followed by polymerisation.

A catalytic transition metal complex will undergo a one-electron oxidation reaction with the halogen in our case immobilised on the surface of the paramagnetic silica.The catalyst reacts with halogen resulting in a radical on the carbon atom, see Figure 2.7A. The equilibrium of this reaction is shifted to the left hand side.

The second step is the polymerisation reaction. The monomer, containing an alkene group, will react with the radical on the surface. The radical will be transferred to a different carbon atom, allowing a continuous growth of the polymer chain. An example is visualised in Figure 2.7B with 2-Hydroxyethyl acrylate as monomer. The reaction will terminate when either all the monomers are consumed or if the system is exposed to air to destabilise the radicals. [15] [16]

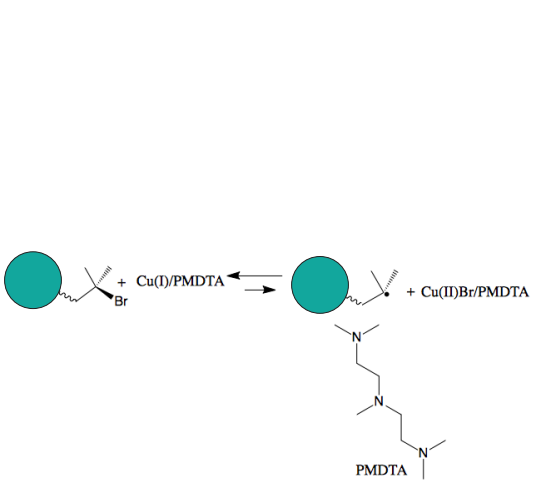

(a) The first step in the ATRP-reaction; the formation of the radical that is connected to the colloidal particle. This reaction is with Copper-N,N,N',N",N"-pentamethyldiethylenetriamine complex as the catalyst and bromine attached to a colloidal particle.

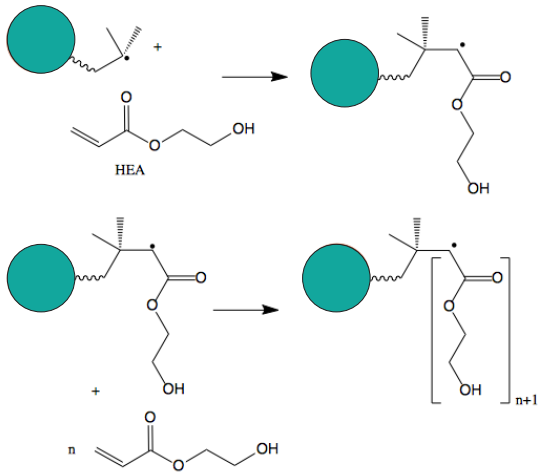

(b) The second step in the ATRP-reaction; the polymerisation of the monomer with the radical that is connected to the colloidal particle.

Figure 2.7: Visualisation of the two steps, a and b, in the atom transfer radical polymerisation reaction with in this case HEA as monomer and the halogen Bromine on the surface of a colloidal particle.

2.6 Radius of Gyration

The radius of gyration is a measure to indicate the approximate size of a polymer. The radius of gyration is dependent on the environment of the polymer. The radius of gyration of poly (ethylene oxide) can be calculated with Equation 2.16 if PEO is in a good solvent [17].

$$R_g = 0.215 M_w^{0.583 \pm 0.031} \text{ nm} \tag{2.16}$$

Chapter 3

Experimental methods

3.1 Materials

Table 3.1: All the chemicals used for the functionalisation steps of superparamagnetic silica spheres.

Name (Abbreviation)	**Purity**	**Supplier**
2 wt% superparamagnetic silica colloids in water, iron oxide >30%, d=0.51 μm, SD=0.03 μm		Micro Particles GmbH
Ethanol	100%	Interchema
Ammonia	25% in water	Fisher
(3-aminopropyl)triethoxysilane (APTES)	$\geq$ 98%	Sigma Aldrich
Tetrahydrofuran (THF)	stabilized with 0.025% BHT	Acros Organics
Triethylamine (TEA)	$\geq$99.5%	VWR
α-Bromoisobutyryl bromide (BIBB)	98%	Sigma Aldrich
Methanol	99.8%	Sigma Aldrich
Copper(I)Bromide (Cu(I)Br)	98%	Sigma Aldrich
2-Hydroxyethyl acrylate (HEA)	96%	Sigma Aldrich
N,N,N',N",N"-Pentamethyldiethylenetriamine (PMDTA)	99%	Sigma Aldrich
Sodium bisulfite		Acros Organics
Dimethylformamide (DMF)	99.8%	Sigma Aldrich
Sodium azide	99%	Fisher
Bromotris(triphenylphosphine)copper	98%	Sigma Aldrich
N,N-Diisopropylethylamine (DIPEA)	$\geq$ 98%	Fluka
Alkyne-coumarin		Ing. K.S. Lacina
Polyethylene oxide (PEO) 6000000 Mv		Sigma Aldrich
2-hydroxy-2-methylpropiophenone (Darocure)	97%	Sigma Aldrich
3-(trimethoxysilyl)propyl methacrylate (TPM)	98%	Sigma Aldrich
Polyethylene oxide (referred to as PEO2) 360 Mn		Sigma Aldrich

All the chemicals used and listed in Table 3.1 are stored in ambient conditions except for the superparamagnetic silica particles and the HEA that was kept in the fridge around $5°C$ and the alkyne-coumarin that was kept in the freezer. The alkyne-coumarin stock solution was made in a ratio 1:3 azide:alkyne-coumarin.

3.2 The Model System

The experimental model system consists of superparamagnetic silica particles in water with polyethylene oxide (PEO) as a depletant. The depletion interaction of -2.51 kT is comparable to the dipolar hard sphere interaction of -2.8 kT. There might be a calculation error in the depletion interaction because the molecular weight is defined in Mv and that might differentiate from the general units of gram per mol. The gravitational length of 2.5 micrometer might be a problem because all the particles could be stuck to the bottom. The model system should be sufficient to experimentally test the simulation of Pickett et al. The results of the simulation are visible in Figure 3.1.

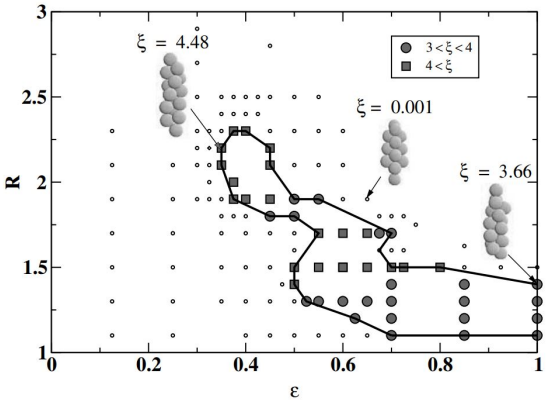

Figure 3.1: The results of the simulation of aligned spherical particles with a dipole moment the presence of an additional attractive interaction. Resulting in different structures dependent on the range of attraction and strength of attraction [6].

The strength of interaction can be found on the x axis and the range of the interaction can be found on the y axis. The strength and range of interaction between the spherical particles are not variables that can be directly used in the lab. The range and strength of the attraction can be varied experimentally by changing the depletion interaction. Therefore it will be useful to convert the axis in practical variables. First the range of attraction will be converted into the radius of the depletant and secondly the strength of attraction will converted into the depletant concentration.

3.2.1 Range of Attraction

The range of attraction, due to depletion interaction, between two colloids is set to be between one and R, where one refers the diameter of the spherical colloids which was set to one in the simulations. The largest distance for R, to still be of significant value, is at the point that the depletion zones start to overlap. The graphical representation of the situation is given in Figure 3.2. A polymer, used as depletant, is a dynamic structure and has a radius of gyration. The range of attraction can be expressed in the unit-less colloids diameter, 1, and radius of gyration,

$$R = 1 + 2R_g. \tag{3.1}$$

The size ratio of the general situation will be equal to the specified case in these calculations and therefore this expression can be rewritten into

$$R = \frac{R_g + R_c}{R_c}. \tag{3.2}$$

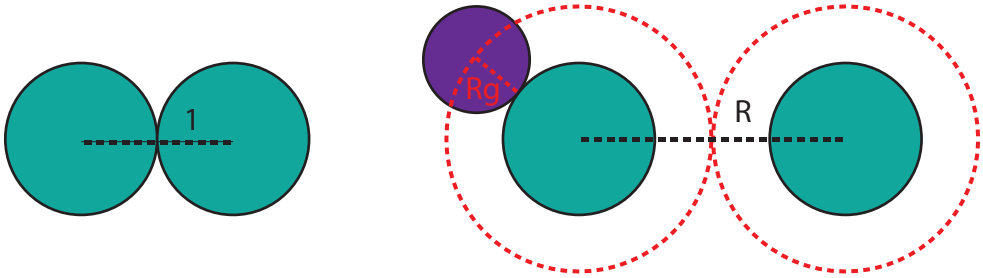

Figure 3.2: A visualisation of two particles in two extremes of the distance in between the particles is minimized (left) or maximized (right) for the depletion interaction.

3.2.2 Strength of Attraction

The strength of the attraction, referred to as the Pickett potential, can be compared to the depletion interaction potential. For ideal polymers the depletion interaction can be calculated with the Asakura-Oosawa-Vrij (AOV) potential [8]. The AOV contact potential, if normalized, can be set equal to the Pickett potential resulting in Equation

$$\phi_d^{bulk} = \frac{2q}{3 + 2q}\epsilon. \tag{3.3}$$

Here, ϵ is the Pickett potential, R_g is the radius of gyration and ϕ_d^{bulk} the relative polymer concentration. The shape of these potentials can be compared to different values of size ratio q, the radius of gyration of the polymer relative to the radius of the colloids. Two situations with different values of q are visualized in Figure 3.3. On the left side q is equal to 0.1 and although the shape of the potentials are different the pair potential does not differ significantly. The situation on the right with a q value of 0.5 also has two different shapes but has larger differences in potential at distances that are not equal to 1 or larger than 1.5. It can be concluded that at a higher q value the difference between the Pickett and AOV potential increases. For a representative experimental model system q should be relatively low. The relative polymer concentration is related to the polymer concentration by Equation

$$\phi_d^{bulk} = \frac{4\pi R_g^3 N_{AV} c}{3M_p} \tag{3.4}$$

[18].

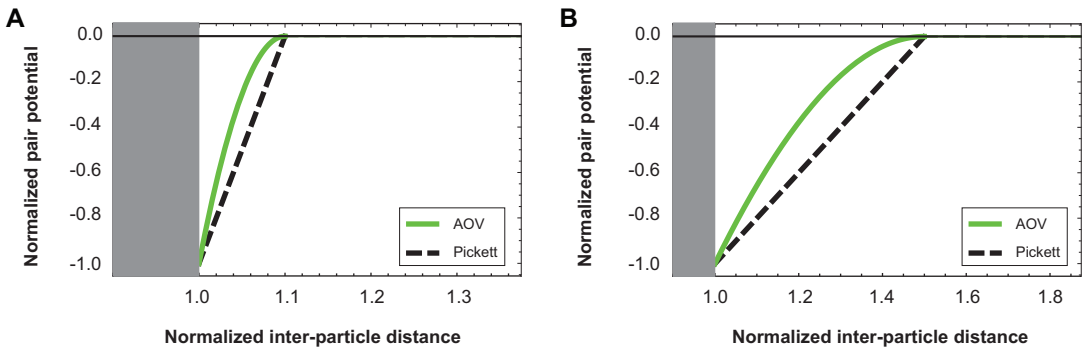

Figure 3.3: Comparison of the Pickett potential and the AOV potential for two different values of q, the radius of gyration of the polymer relative to the radius of the colloids. q has a value of 0.1 (left) and a value of 0.5 (right).

3.2.3 New Phase Diagram

The strength of the attraction and the range of the attraction can be converted into functional variables. The phase diagram by Pickett et al. can be converted into Figure 3.4, where the axis represent the radius of gyration and the packing fraction.

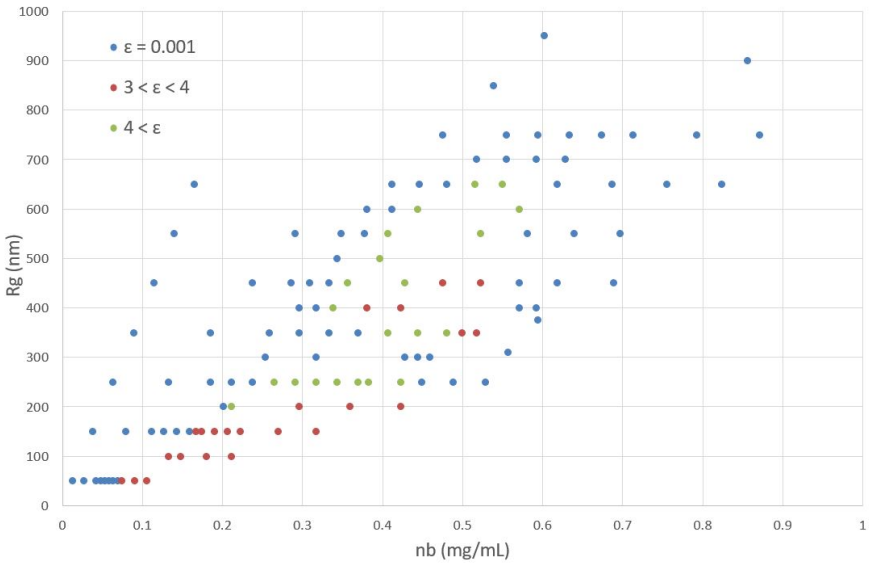

Figure 3.4: The phase diagram with the results of the simulations adapted with the range of the attraction into the radius of gyration and the strength of the attraction into the depletant concentration.

3.3 Helmholtz Cube

A uniform homogeneous magnetic field can be created with a set up of a pair of round Helmholtz coils of equal size at a distance of each other equal to the radius of the coils. The strength of the magnetic field can be calculated with

$$B = \frac{8\mu_o}{5\sqrt{5}R} I, \tag{3.5}$$

where μ_0 equals the permeability in free space, I the current magnitude and R the radius of the coil. The Helmholtz cube consists of three Helmholtz pairs that are arranged

orthogonally as can be seen in Figure 3.5. This cube is able to create a three-dimensional homogeneous magnetic field. There is one pair of round coils and two set of square coils. The square coils are positioned at a distance apart, equal to 0.5445 times the length of the square sides. The magnetic field strength can be calculated with

$$\mathbf{B}(\mathbf{r}) = \frac{\mu_0}{4\pi} I \oint \frac{d\mathbf{l}' \times \hat{\mathbf{r}}}{r^2}, \tag{3.6}$$

with integration along the current path that carries the current I and the vector **r** defined as the distance from the source to the field observation point r. The uniformity of the square Helmholtz coils is defined within a deviation of 0.5% of the local vector field compared to the magnetic field strength in the center in between the coils. This unifomity is visualized in Figure 3.6 for two square coils 48 mm apart and the point 0, 0, 0 in the centre. The properties of the Helmholtz cube at a maximum current of 1.55 Ampère are given in Table 3.2. This is the maximum current for this cube with copper round wires with a diameter of 0.71 mm with no forced cooling. [19]

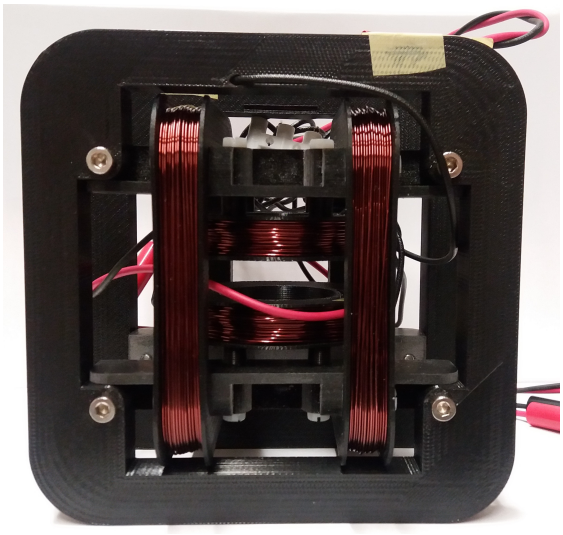

Figure 3.5: A picture of the Helmholtz cube, where three sets of coils are visible so a magnetic field in all direction can be applied.

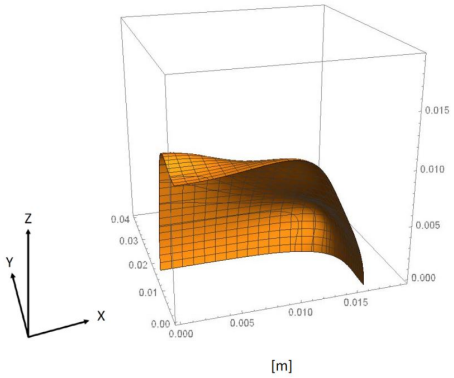

Figure 3.6: A visualisation of the uniformity of two square coils 48 mm apart and the 0, 0, 0 in the centre.

Coil pair	Field Direction B	Geometry coil	Turns	| **B** | (mT)
Inside	Z	Circular	170	6.2
Middle	Y	Square	140	3.2
Outside	X	Square	170	3.2

Table 3.2: Properties of the Helmholtz cube at a maximum current of 1.55 A.

3.4 Debye Screening Length

The Debye screening length is the distance from the charged colloidal particle where the influence of the electric charge of the colloid is significantly small [20]. A reduction of the Debye screening length will make sure that the particles can come close enough together and not interfere to much with the depletion interaction and magnetic moment. The Debye screening length was reduced to 3 nm, since at this length the coulomb repulsion

between charged colloids is reduced to let colloids interact at small distances, but keeps the colloidal dispersion stable. The corresponding salt concentration can be calculated with

$$\kappa^{-1} = \frac{0.304}{\sqrt{I}}. \tag{3.7}$$

Here, κ^{-1} is the Debye screening length and I is the salt concentration in the bulk. This equation is only valid for monovalent salts at 25 ^oC in water. The concentration of salt needed for a Debye screening length of 3 nm is 10 mM. [9]

3.5 Functionalisation of Superparamagnetic Colloids

In order to attach coumarin to the surface of the superparamagnetic silica, five functionalisation steps are needed. An overvieuw of all the functionalisation steps can be seen in Figure 3.7.

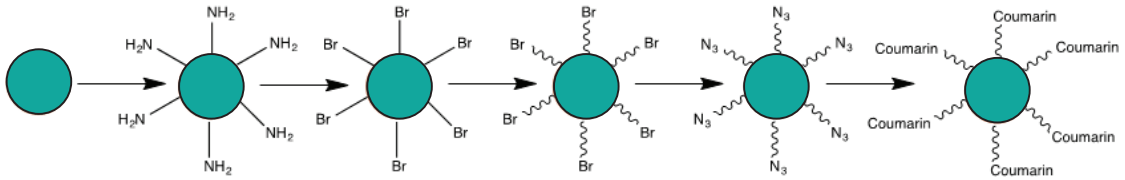

Figure 3.7: An overvieuw of all the functionalisation steps of the superparamagnetic silica; amine functionalisation, bromine functionalisation, ATRP-reaction, azide functionalisation and coumarin functionalisation.

3.5.1 Amine-functionalisation

400 μL 2.5 wt% superparamagnetic silica particles were washed (4722g, 2 min) three times with ethanol and redispersed in 1 mL water. The colloidal dispersion was sonicated for at least 30 minutes before the dispersion was placed in an oil bath of 60°C and stirred with a magnetic stirrer. Subsequently 6 μL ammonia, 0.5 mL 10 V% APTES in ethanol and 0.5 mL ethanol were added to the dispersion; only the APTES solution was added drop by drop. The dispersion was stirred in the oil bath for approximately 20 hours. The dispersion was washed(4722g, 2 min) three times with ethanol.

3.5.2 Bromine-functionalisation

The colloids, now amine-functionalised, were washed (4722g, 2min) three times with THF and redispersed in 1 mL THF. The colloidal dispersion was placed in a sonication bath for at least 30 minutes before placing the dispersion in an ice bath while stirring magnetically. 30.4 μL triethylamine and 23.5 μL BIBB were added. The mixture remained in the ice bath while being stirred at least 30 minutes followed by approximately 20 hours stirring without ice bath. The dispersion was washed (4722g, 2 min) three times with THF.

3.5.3 ATRP Reaction

The bromine-functionalised colloids were washed (3615g, 2 min) with 7:3 (v:v) methanol:water mixture and redispersed in 0.5 mL 7:3 (v:v) methanol : water mixture. The colloidal dispersion was sonicated for at least 30 minutes before the dispersion was placed in a Schlenk flask. In a different Schlenk flask with magnetic stirrer, 6.9 mg Cu(I)Br was partially dissolved in 0.5 mL 7:3 (v:v) methanol : water mixture. 69 μL HEA was added to the

Schlenk flask with the Cu(I)Br solution. Both Schlenk flasks were degassed and flushed with nitrogen three times. 29 μL PMDTA was added to the Schlenk flask with the Cu(I)Br solution quickly without stirring. The obtained Cu(I)Br mixture was quickly degassed and flushed with nitrogen. The colour was an indicator if the reaction was successful, where dark blue indicated failure and blue/green indicated a successful reaction. The colloidal dispersion was added under inert conditions. The reaction was left stirring for 1 hour before exposure to air. The colloids were washed (3615g, 2 min) three times with 7:3 (v:v) methanol : water mixture, 10 times with 50 mM aquous $NaHSO_3$, 2 times with ethanol, 3 times with water and finally redispersed in 1 mL water.

3.5.4 Azide-functionalisation

The colloids, 1 wt% resipered in 1 mL water now with HEA polymer brushes on the surface, were washed three times with DMF and redispersed in 0.5 mL DMF. The dispersion was sonicated for at least 30 minutes before the dispersion was added to a solution of 9 mg NaN_3 in 1.5 mL DMF. The dispersion was placed in a oil bath at 60°C while stirring for 24 hours. The colloids were washed 3 times with DMF and redispersed in 1 mL DMF.

3.5.5 Coumarin-functionalisation

12.5 mg Bromotris(triphenylphosphine)copper was dissolved in 1 mL of DMF in a Schlenk-flask while stirring magnetically. 26 μL DIPEA and 1 mL of alkyne coumarin stock solution was added to the Schenk flask. 0.5 mL of the 1 wt% azide functionalised colloids were added to the Schlenk-flask. The Schlenk-flask with the colloidal dispersion was stirred for 24 hours in an oil bath at 70 °C. The coumarin-functionalised colloids were washed three times with DMF, three times with DMF and redispered in 0.5 mL water.

3.6 Characterisation Techniques

3.6.1 Infra-red Spectroscopy

A Perkin Elmer FT-IR/FIR Frontier Spectrometer was used to record IR-spectra between 4000 and 650 cm^{-1} with steps of 4 cm^{-1}. The IR-spectra were prepared from a drop of colloidal dispersion in water dried in air.

3.6.2 Transmission Electron Microscopy

A Philips TECNAI 10 TEM was used to obtain TEM images. The TEM samples were prepared by placing a drop of dilute dispersion of superparamagnetic silica spheres on a copper grid with a polymer layer. The TEM grids were dried with the use of a heat lamp. The size of the colloids was determined by measuring the average of 150 particles.

3.6.3 Scanning Electron Microscopy

The FEI XL30 FEG scanning electron microscope operating at 5-15 kV was used to image the colloids after the coumarin functionalisation. The SEM samples were prepared by drying a drop of diluted coumarin functionalised superparamagnetic particles on a TEM grid with a heat lamp.

3.6.4 Optical Microscopy

A Nikon Eclipse Ti-U optical microscope was used to analyse the samples. The microscope was equipped with 20x objective, 40x objective and a 60x oil objective. All the samples

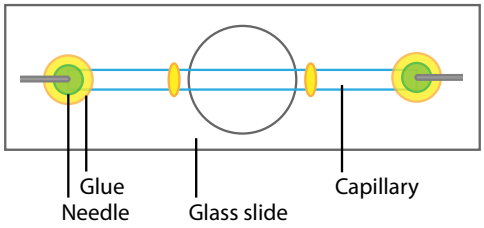

(a) A schematic representation of the flow cell used.

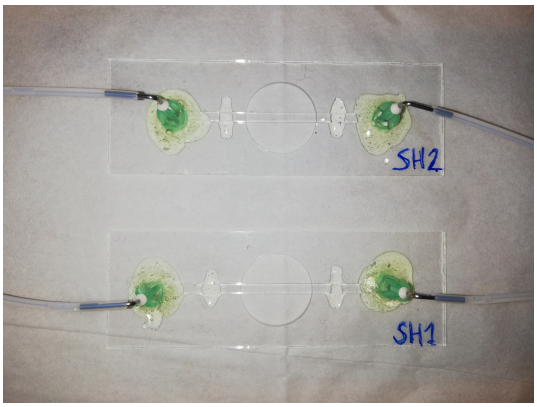

(b) Image of the flow cells used.

Figure 3.8: Visualisation of the flow cells and its components.

used for the microscope experiments were made by preparing a mixture of 600000 M_v PEO stock, water with salt and superparamagnetic particles stock (1 wt%). The formed samples all contain a concentration of 0.05 wt% superparamagnetic colloids and a salt concentration of 10 mM. Both NaCl and NaN_3 were used as salt. The concentration of PEO was varied.

Most optical microscopy samples were made with a capillary of 0.1 mm by 2.0 mm and UV glue. Some capillaries were coated with polymer hairs to prevent sticking of the particles to the glass. This required a different optical microscopy sample namely a flow cell, see in Figure 3.8.

Capillary Coating

A capillary in the setup as shown in figure 3.8 was filled with 2 M NaOH for 5 minutes. The capillary was rinsed with water followed by ethanol. A mixture of 800 μL ethanol, 20 μL ammonia and 20 μL TPM. This mixture was left in the capillary for at least one hour. The sample was rinsed with ethanol and left to dry in nitrogen flow overnight. A mixture of 2.5 mL ethanol, 500 μL HEA or PEO2 and 20 μL Darocure was injected into the capillary. The capillary was placed under UV light for 14 minutes. The capillary was rinsed with water extensively and the capillary was left with water inside until it was used.

The Coumarin Functionalised Optical Microscopy Samples

The superparamagnetic silica spheres functionalised with coumarin samples were made two different ways. The first samples were made as a 0.05 wt% in water. The other set of samples were made of 0.05 wt% in ethanol water mixture. The exact compositions are specified with the results.

Chapter 4

Results and Discussion

4.1 Synthesis of Photoresponsive Colloids

The functionalisation of superparamagnetic silica colloids was monitored with IR. The size and shape of the particles were analysed with TEM and SEM.

4.1.1 Infra Red Spectroscopy

IR-spectra were taken after the following functionalisations; ATRP-reaction, azide-functionalisation and the coumarin-functionalisation. Figure 4.1 contains the IR-spectra indicating successful functionalisations. These functionalisations modify the IR spectrum in such a way that confirmation is possible. A successful ATRP-reaction is indicated with a sharp peak visible around 1700 cm^{-1} from the double bond between the carbon and oxygen in HEA. The azide functionalisation gives a peak at of around 2100 cm^{-1}. The coumarin functionalisation decreases that azide peak because the azide shifts in formation when it reacts with coumarin.

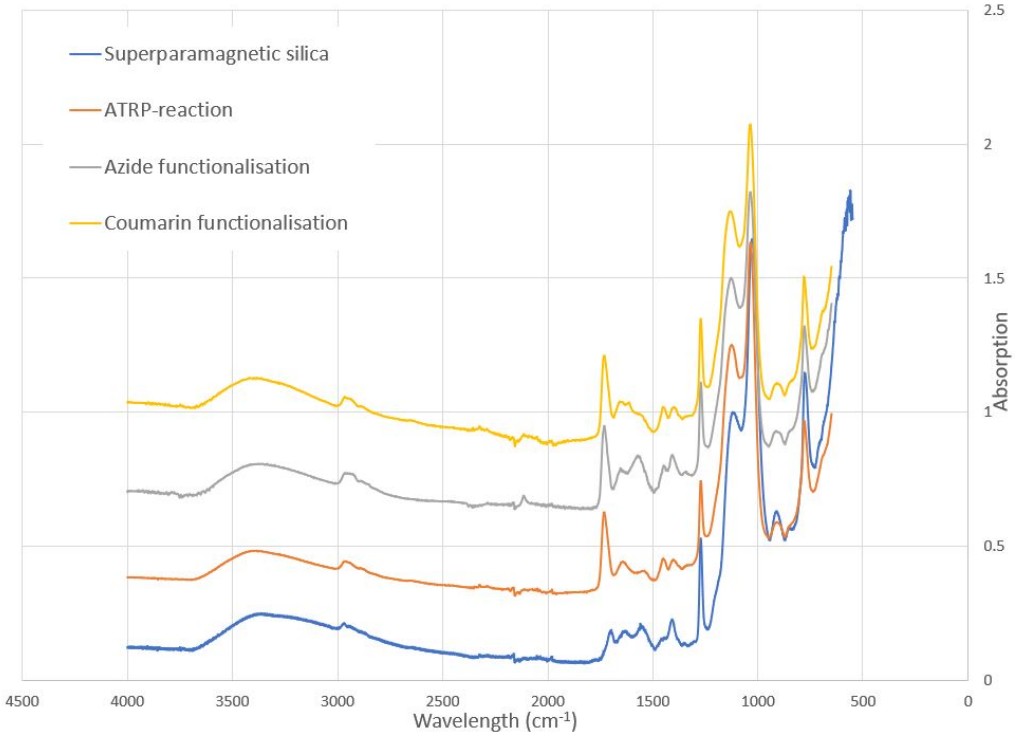

Figure 4.1: IR spectra of superparamagnetic particles before and after ATRP-reaction, azide-functionalisation and coumarin-functionalisation.

4.1.2 Transmission Electron Microscopy

Transmission electron microscopy was used to determine the size of the superparamagnetic silica particles. The size of the particles was measured for 157 particles resulting in a mean size of 522.1 nm with a standard deviation of 16.2 nm. The maximum size measured was 593.0 nm and the minimum size measured was 504.7 nm. A representative TEM image can be seen in Figure 4.2.

4.1.3 Scanning Electron Microscopy

Scanning electron microscopy was used to look at the surface of the coumarin functionalised particles. In Figure 4.3 a SEM image can be seen. The image shows a lot of smooth particles but two of them are broken. This could be due to the mechanical force of stirring with the magnetic stirrer or the sonication bath.

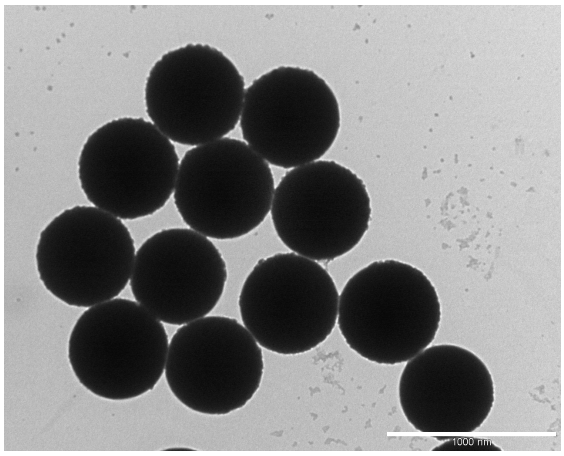

Figure 4.2: A representative TEM image of superparamagnetic silica particles.

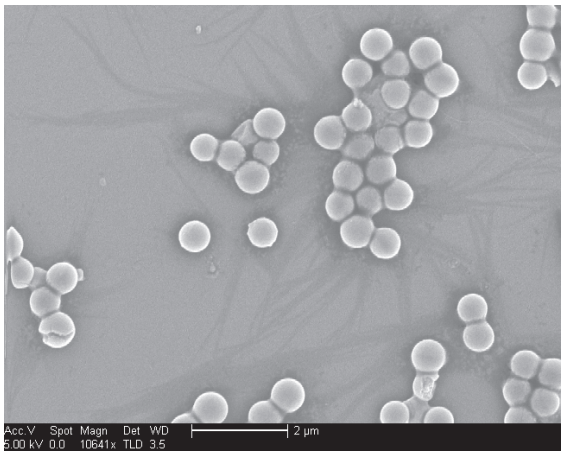

Figure 4.3: A representative SEM image of a coumarin functionalised superparamagnetic silica.

4.2 Spheres in a magnetic field

The next part will discuss the results of the spherical particles in magnetic field where different concentrations of PEO were used.

4.2.1 Superparamagnetic spheres in a magnetic field of 3.4 mT

The behaviour of the superparamagnetic silica spheres were analysed at different polymer concentrations in a horizontal magnetic field of 3.4 mT. The behaviour of a sample varies over time because superparamagnetic spheres in a constant magnetic field are in a dynamical equilibrium. The samples were left in a magnetic field for one hour before analysis of the formed structures, see Figure 4.4. The length of the chains would not change significantly after that time, but they still show Brownian motion. Leaving a sample shorter than one hour, the chains might still be in the process of forming chains. Mainly single linear and sometimes double linear chains are present in the sample after addition of the polymer. No chiral structures were observed for this field strenght. The reason why no helical structure were observed, might be the strength of the magnetic field. The double chains are mostly present in the middle of the structures. This means that in case the chains wrap around each other the length of this chiral structure would be shorter than two chains next to echother and the top and bottom part of the chain would have to move.

This could be an energy penalty that will decrease the chance of the formation of chiral structures. Another reason chiral structures might not be present is that the depletetion interaction might not be strong enough to compete with this magnetic moment. That is why a lower magnetic field was also tested.

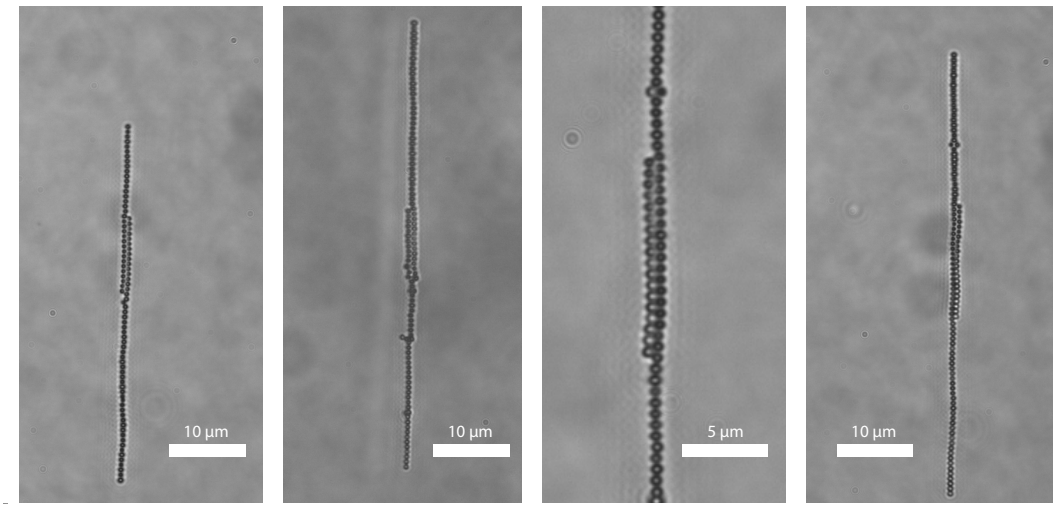

Figure 4.4: From left to right 0.05 wt% superparamagnetic silica particles with 0 mg/ml, 0.10 mg/ml, 0.14 mg/ml and 0.16 mg/ml PEO after one hour in a horizontal magnetic field of 3.4 mT.

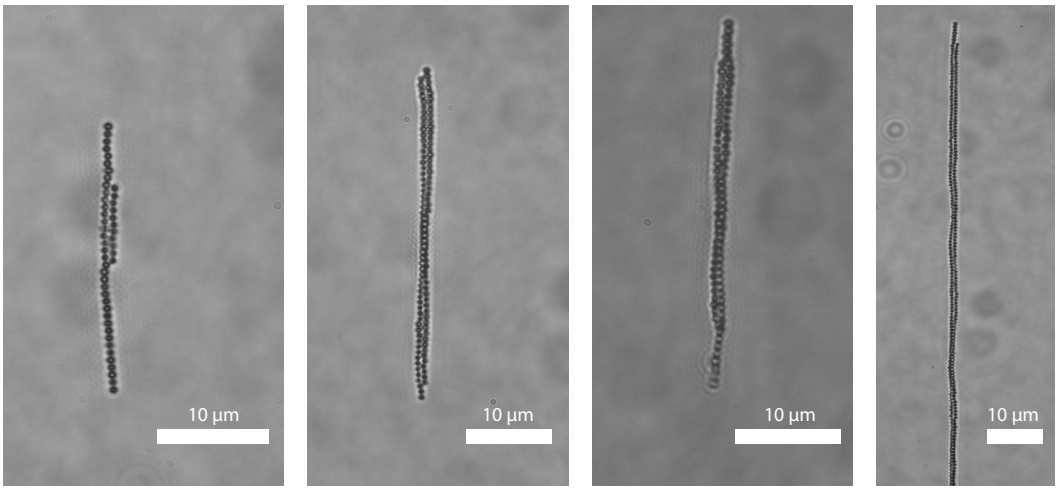

Figure 4.5: From left to right 0.05 wt% superparamagnetic silica particles with 0 mg/ml, 0.10 mg/ml, 0.14 mg/ml and 0.16 mg/ml PEO after one hour in a horizontal magnetic field of 1.4 mT.

4.2.2 Superparamagnetic spheres in a magnetic field of 1.4 mT

The behaviour of the superparamagnetic silica spheres was analysed at different polymer concentrations in a horizontal magnetic field of 1.4 mT, see Figure 4.5. The Figure represents structures found in the samples with a polymer concentration from 0.10 mg/ml to 0.16 mg/ml. Clearly the influence of the added polymer can be seen. The chains twist around each other over time. Comparing the results of both magnetic field strengths,

the strength of the magnetic field influences the chain length. Longer chains are formed at a higher magnetic field with and without added depletant. The lower magnetic field allows the formation of relative short chains that twist around each other when depletant is added.

4.3 Coumarin functionalised particles

The structures visible in Figures 4.4 and 4.5 are dynamic and if you remove the magnetic field the structures will fall apart into separate particles. To fixate the chiral structures and form permanent helical structures, the particles were functionalised with coumarin and placed under UV light in a magnetic field.

4.3.1 Click Reaction in Water

Superparamagnetic particles functionalised with coumarin redispersed in water in an external magnetic field of 3.4 mT and in the presence of PEO were irradiated with UV light. After 24 hours, no photo-dimerization appeared to have taken place apart from some clusters that were also present in the control sample, see Figure 4.6. The control sample is a representative sample in the same environment except that it is not exposed to UV light. The UV light was blocked by aluminum foil. A test of the functionality of coumarin with IR spectroscopy, not shown, indicated that the coumarin was still active in ethanol. Due to that fact the same experiment was done in an ethanol water mixture.

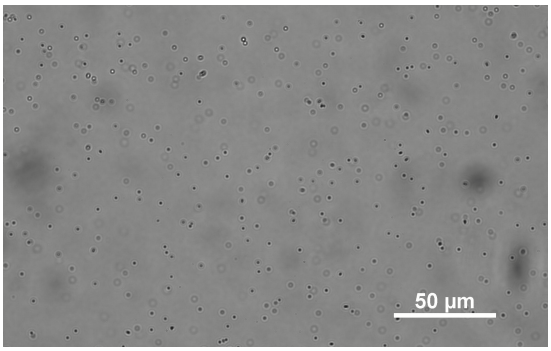

(a) The sample before exposure to a magnetic field and UV light.

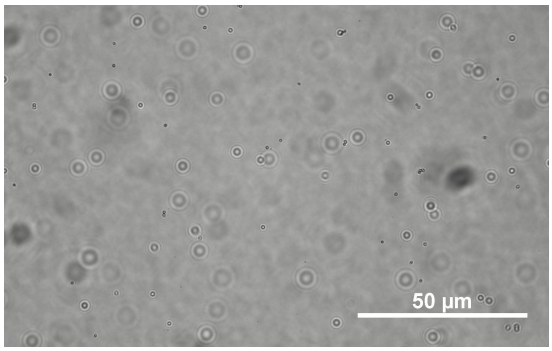

(b) The sample after exposure to a magnetic field and UV light.

Figure 4.6: Optical microscopy images of coumarin functionalised silica spheres before and after exposure to a horizontal magnetic field of 3.4 mT and UV light for 24 hours.

4.3.2 Click Reaction in a Water Ethanol Mixture without Depletant

Coumarin functionalised particles in ethanol water mixture (0.5 v% water) after exposure to a magnetic field of 3 mT and UV light for 65 hours are visible in Figure 4.7. The chains are permanently bonded together without the magnetic field, see Figure 4.7a. Figure 4.7b shows one of these chains in detail. The colloidal particles in the chain are not perfectly horizontally aligned, this could be due to the fact that the ethanol water mixture is not the ideal environment for these particles. It is not ideal because the functionalised particles, due to the HEA polymer chains on the surface, are not stable in pure ethanol. Cluster are therefore more prone to exist in these samples. Figure 4.7c shows that the sample contains clusters that will align in a chain giving these cluster chain like kinds of structures. At the side of the capillaries single particles were found, see Figure 4.7d. This might be because the particles are shielded by the Helmholtz cube from UV light or the UV glue interacts with the sample.

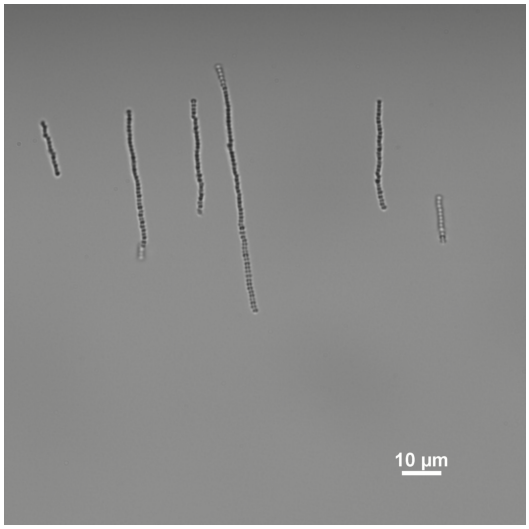

(a) Overview of the structures.

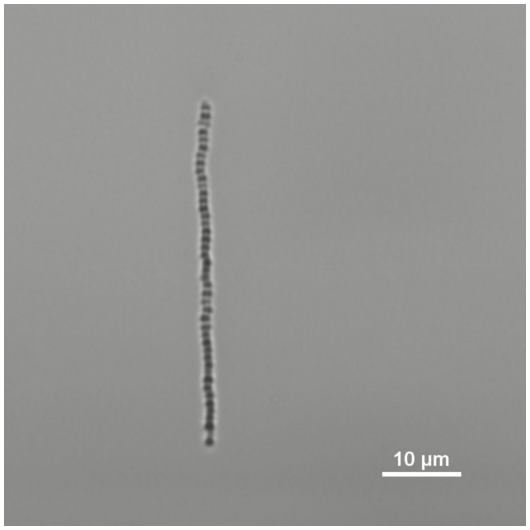

(b) A straight chain.

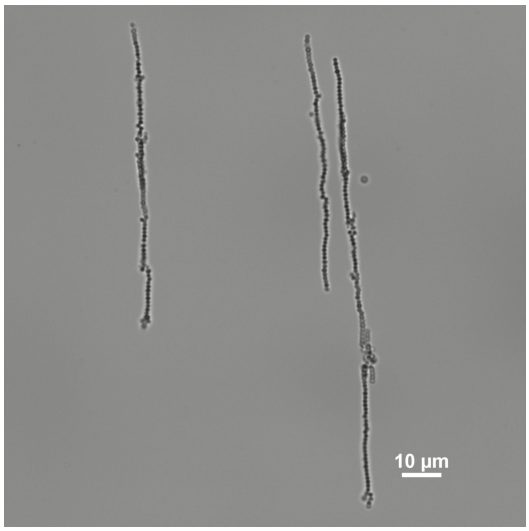

(c) Clusters in the sample embedded into the chain formation.

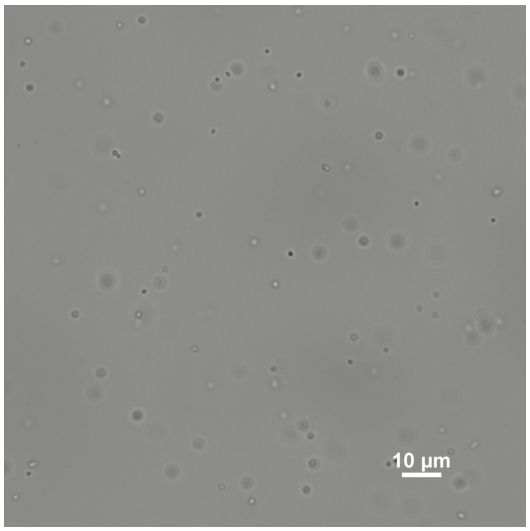

(d) Single particles present at the end of the capillary.

Figure 4.7: Optical microscopy images of a sample with depletant in a magnetic field of 3.4 mT after exposure to UV light for 65 hours. In this sample the chains are nicely aligned because a small magnet was placed next to the sample.

4.3.3 Click Reaction in a Water Ethanol Mixture with Depletant

Coumarin functionalised particles in ethanol water mixture (14.5 v% water) with a PEO concentration of 0.14 mg/ml after exposure to a magnetic field of 3.4 mT and UV light for 65 hours are visible in Figure 4.8. In Figure 4.8a an overview of the formed chains are visible, where b gives a closer look of the straight chains that was formed. These obtained clusters were shorter than the structures seen and expected in Figure 4.5. Clusters are also embedded into the chains, this can be seen in c. At the end of the capillary again loose particles were present, see d. Shorter capillaries were used but to no avail. The experiment was repeated with a lower magnetic field of 1.4 mT, only the UV-glue was exchanged for two component glue. Different glue was used to exclude the idea that the glue might interfere with the click reaction at the ends of the capillary. The results are visible in Figure 4.9. In Figure 4.9a an overview of the found structures are visible. There are a lot of different structures present in the sample. In Figure 4.9b two chains connected at one

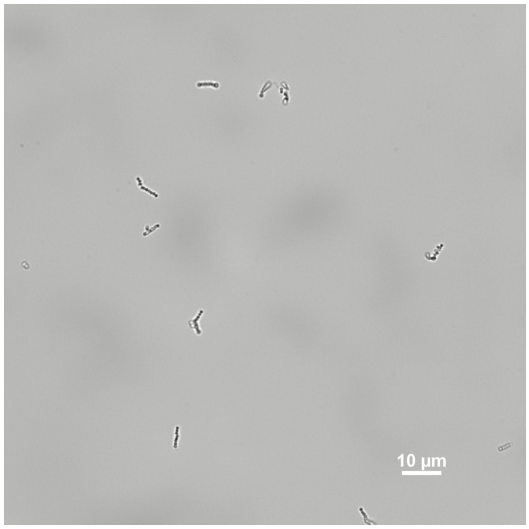

(a) Overview of structures.

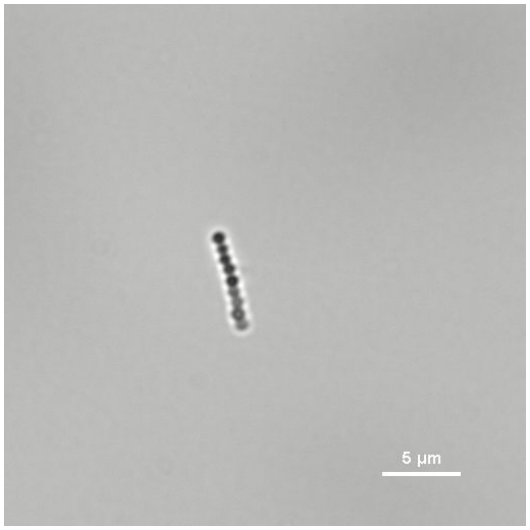

(b) A straight chain.

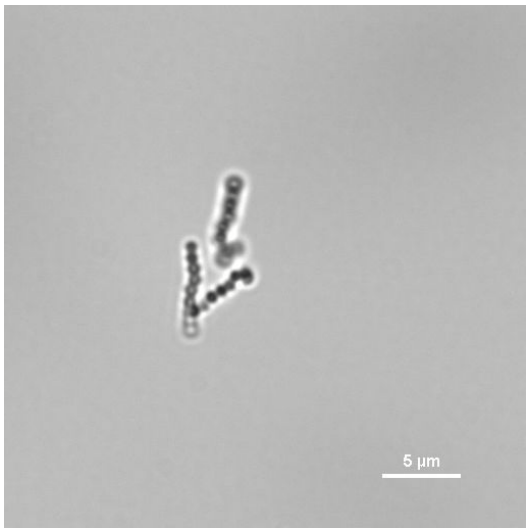

(c) Clusters in the sample embedded into the chain formation.

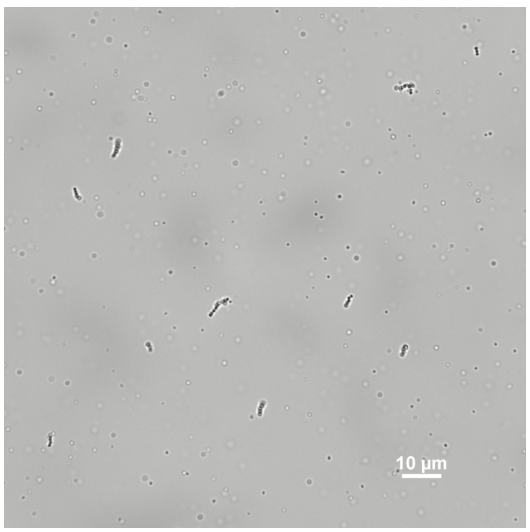

(d) Single particles present at the end of the capillary.

Figure 4.8: Optical microscopy images of a sample with depletant in a perpendicular magnetic field of 3.4 mT after exposure to UV light for 65 hours.

point can be seen. This structure could have been a helical shape when the magnetic field was applied. The efficiency of the coumarin click reaction could have been decreased in such a way that the only a part of the structure was fixated. This could also explain why the obtained chains are shorter than expected. In Figure 4.9c a structure is visible that could be chiral. It is difficult to determine the three dimensional structure because with the optical microscope only two dimensional images are obtained. Therefore, clusters as in d are difficult to analyze. No single particles were found at the end of the capillary, due to the fact that instead of UV glue, two-component glue was used.

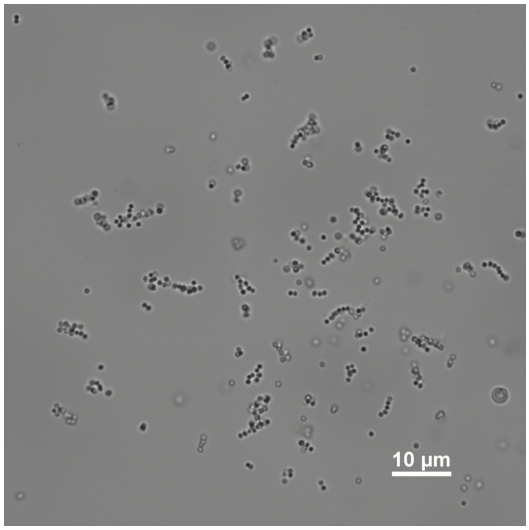

(a) Overview of the structures.

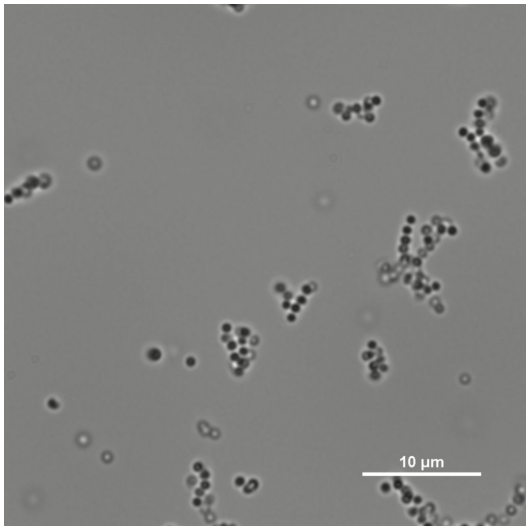

(b) A closer look at the sample.

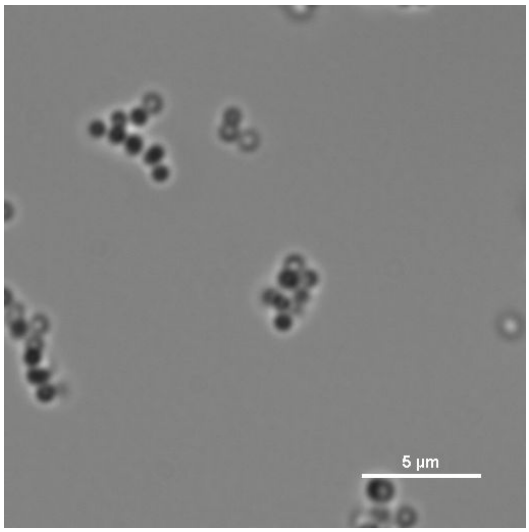

(c) A possible helical structure.

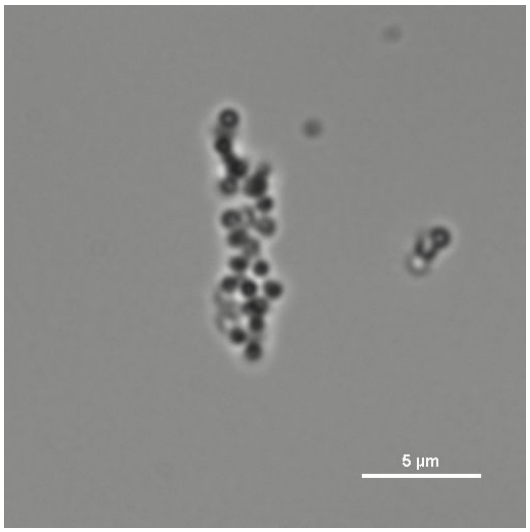

(d) Large cluster with undefined structure.

Figure 4.9: Optical microscopy images of a sample with depletant in a magnetic field of 1.4 mT after exposure to UV light for 65 hours.

Chapter 5

Conclusions and Outlook

Superparamagnetic silica colloids were analyzed at different circumstances. The particles formed straight chains in a homogeneous magnetic field. The strength of the magnetic field influences the chain length. A lower magnetic field strength results in shorter chains. Different effects of the addition of PEO were seen at two magnetic field strengths. At a magnetic field of 3.4 mT the addition of polymer up to 0.16 mg/ml did not have a significant influence on the formed structures but will increase the chain length. At a magnetic field of 1.4 mT the addition of polymer lead to the formation of double chains who twist around each other.

The superparamagntic silica particles were successfully functionalised with coumarin through a five step synthesis; amine-functionalisation, bromine-functionalisation, ATRP-reaction, azide functionalisation and coumarin-functionalisation. The synthesis of the functionalised particles was successful as confirmed by IR. The coumarin functionalised particles did not click together in water after exposure to UV-light in a magnetic field for 65 hours. Changing the medium to a water ethanol mixture appeared crucial for the coumarin click reaction. The coumarin click reaction was successful and provided permanent structures of the supermagnetic particles. The only result that was obtained the 1.4 mT with depletant present with obtained structures that were shorter than expected.

The loss of functionality of the coumarin, even in optimal storing conditions, is problematic. As an outlook a different mechanism for the fixation of the structure could be used. The use of newly synthesized coumarin might be optimal to reproduce these results in a water. Both of these experiment would be interesting to confirm the obtained results. The eventual chiral structures could be used as a model system for DNA. This model system could be exposed to different conditions to analyse it behaviour. The chirality of the final structures could be analysed with an polarimeter to determine if left or right handed chiral structures were present [21]. Maybe tuning of one handed chiral structures could be possible. Another application might be the creation of a liquid crystal that is responsive to a magnetic field. Different liquid crystals could be formed with rod like structures and chiral structures. After careful analysation of their exact properties new functions could be discovered. These new functions could be useful in the production of new interesting materials or devices.

Bibliography

[1] C. Bernardini, S. Stoyanov, L. Arnaudov, and M. Stuart. Colloids in flatland: A perspective on 2D phase-separated systems, characterisation methods, and lineactant design. *Chemical Society Reviews*, 42(5):2100–2129, 2013.

[2] V. Manoharan. Colloidal matter: Packing, geometry, and entropy. *Science*, 349(6251):1253751, 2015.

[3] Lord Kelvin. The second robert boyle lecture. *Oxford Univ. Junior Scientific Club*, 18:25, 1894.

[4] J. Yan, M. Bloom, S. Bae, E. Luijten, and S. Granick. Linking synchronization to self-ssembly using magnetic Janus colloids. *Nature*, 491(7425):578, 2012.

[5] D. Zerrouki, J. Baudry, D. Pine, P. Chaikin, and J. Bibette. Chiral colloidal clusters. *Nature*, 455(7211):380, 2008.

[6] G. Pickett, M. Gross, and H. Okuyama. Spontaneous chirality in simple systems. *Physical Review Letters*, 85(17):3652, 2000.

[7] P. van Vliet. Chiral structures from simple isotropic colloids using depletion interaction. *Bachelor Thesis*, 2016.

[8] H. Lekkerkerker and R. Tuinier. *Colloids and the depletion interaction*, volume 833. Springer, 2011.

[9] J. Israelachvili. *Intermolecular and surface forces*. Academic press, 2011.

[10] A. Philipse and B. Kuipers. Second virial coefficients of dipolar hard spheres. *Journal of Physics: Condensed Matter*, 22(32):325104, 2010.

[11] P. Liu. Self-assembly of magnetic colloids in soft confinement. *PhD Thesis*, 2016.

[12] S. Buzzaccaro, A. Tripodi, R. Rusconi, D. Vigolo, and R. Piazza. Kinetics of sedimentation in colloidal suspensions. *Journal of Physics: Condensed Matter*, 20(49):494219, 2008.

[13] J. Meijer, A. Pal, S. Ouhajji, H. Lekkerkerker, A. Philipse, and A. Petukhov. Observation of solid–solid transitions in 3D crystals of colloidal superballs. *Nature Communications*, 8:14352, 2017.

[14] A. Darras, E. Opsomer, N. Vandewalle, and G. Lumay. Superparamagnetic colloids in viscous fluids. *Scientific reports*, 7(1):7778, 2017.

[15] K. Matyjaszewski and J. Xia. Atom transfer radical polymerization. *Chemical Reviews*, 101(9):2921–2990, 2001.

[16] J. Wang and K. Matyjaszewski. Controlled/" living" radical polymerization. atom transfer radical polymerization in the presence of transition-metal complexes. *Journal of the American Chemical Society*, 117(20):5614–5615, 1995.

[17] K. Devanand and J. Selser. Asymptotic behavior and long-range interactions in aqueous solutions of poly (ethylene oxide). *Macromolecules*, 24(22):5943–5947, 1991.

[18] S. Ouhajji. Surface adsorption versus bulk aggregation of stearyl-coated silica spheres and surfaces. *Master Thesis*, 2013.

[19] B. Kuipers. Theory helmholtz coils. Technical report, Utrecht University, 2018.

[20] U. Nobbmann. Debye screening - how it effects zeta potential, 2018. `https://www.materials-talks.com/blog/2018/10/03/debye-screening-how-it-affects-zeta-potential/`.

[21] A. De Martino, Y. Kim, E. Garcia-Caurel, B. Laude, and B. Drévillon. Optimized mueller polarimeter with liquid crystals. *Optics letters*, 28(8):616–618, 2003.

Appendix A Big Spheres

Larger particles are easier to visualize with an optical microscope. The previously mentioned experiments were also preformed with larger particles of 970 nm, which will be referred to as big spheres. The big spheres are distinguishable from each other when aligned in a magnetic field. As a reference, in Figure 5.1 the small particles and the big particles can be seen.

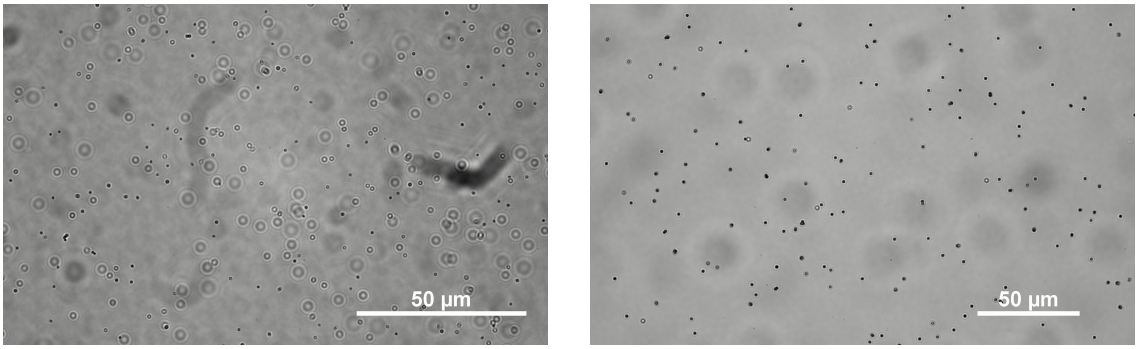

Figure 5.1: Left to right, small and big superparamagnetic silica particles of 510 nm and 970 nm.

Experimental

Samples were prepared containing 0.05 wt% super paramagnetic big silica particles and 10 mM salt. The prepared samples were analysed with the Nikon eclipse Ti-U optical microscope in different setups. The set up for adding in depletant depletant 0.5 mL 200000 Mv PEO solution of 2 mg/mL was used.

Optical Microscopy Set Ups

Two kinds of setups were used to analyse the big spheres. The first set up is a classical optical microscopy sample see Figure 5.2a. To be able to monitor the structure of the chains while adding depletant in situ a set up as in Figure 5.2 B was used.

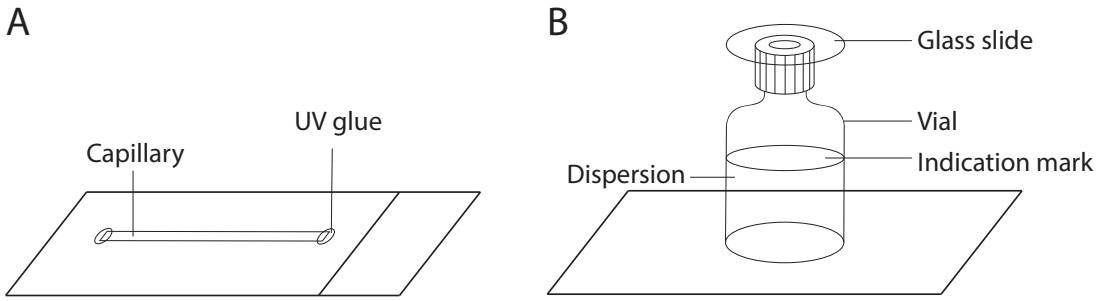

Figure 5.2: The two setups used to analyse the big spheres with optical microscopy. On the left a standard sample and on the right a set up to add the depletant in situ where the indication mark is at the top of the meniscus.

Results and Discussion

The formation of small rods would be useful to form a model system for the simulation where the system consists of 15 hard spheres [6]. The length of these rods can be slightly tuned toward shorter rods by doing the following. Firstly, a magnetic field is applied perpendicular to the sample. This will allow rods to form the height of the capillary and/or the gravitational penalty will ensure that the chains can not grow indefinitely. Then an orthogonal magnetic field is slowly applied followed by the slowly switching off for the perpendicular magnetic field. The results for this technique shows a shorter chain length than by simply applying a magnetic field orthogonal, see Figure 5.3.

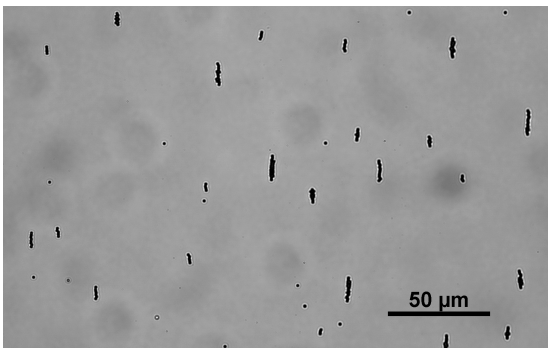

(a) The method to produce shorter rods by firstly equilibrating the sample in a magnetic field perpendicular to the sample followed by turning them into the orthogonal magnetic field.

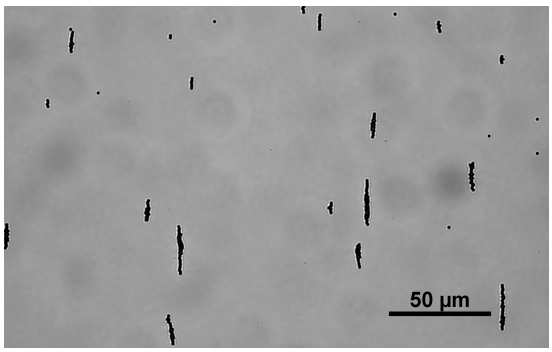

(b) The sample after exposure to a horizontal magnetic field.

Figure 5.3: Optical microscopy images of the big superparamagnetic silica spheres in a magnetic field.

The addition of PEO solution while the super paramagnetic big silica spheres are already aligned in a magnetic field added more complications than benefits. The set-up will allow all the particles to sink to the bottom and display a very high local concentration. The addition of polymer solution with a needle is relatively hard to manage in the current set up without interfering with the image that the microscope displays and touching the glass set-up. The other difficulty arises from the addition of the extra liquid. Most drops that fall into the vial will disrupt the formed structure of the super paramagnetic spheres, see Figure 5.4. The last problem that was encountered, was the large amount of particles that where stuck to the glass after the addition of PEO and the magnetic field that was

turned off. The addition of PEO from above pushed them on the glass.

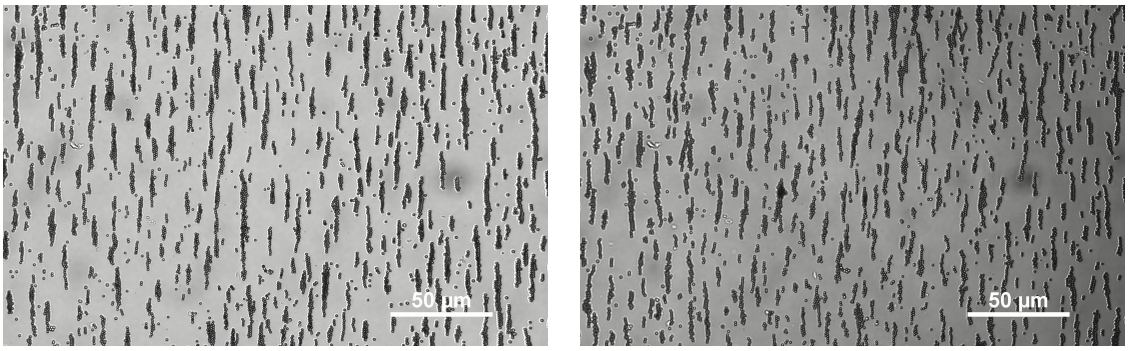

Figure 5.4: From left to right, optical microscopy images of the big superparamagnetic silica spheres in a magnetic field before and after addition of a PEO solution.